East European Journal of Physics. 1. 531–539 (2026)
DOI: 10.26565/2312-4334-2026-1-61 ISSN 2312-4334

IMPACT OF BARIUM DOPING ON THE STRUCTURAL AND OPTICAL PROPERTIES OF NiO THIN FILMS

Mohamed Begui[1*], **Mebrouk Ghougali**[1,2]
[1]*Faculty of Exact Sciences, Photonics Group, Renewable Energy Development Research Unit in Arid Zones (UDERZA), University of El Oued, El Oued, Algeria*
[2]*Faculty of Exact Sciences, LEVRES Laboratory, University of El Oued, 39000 El Oued, Algeria*
[*]*Corresponding Author e-mail: Begui-mohamed@univ-eloued.dz*
Received December 12, 2025; revised February 9, 2026; accepted February 25, 2026

This study investigates the influence of barium (Ba) doping on the structural and optical properties of nickel oxide (NiO) thin films synthesized via spray pyrolysis . NiO films with Ba concentrations of 0%, 2%, 4%, 6%, and 8% were analyzed using XRD, FT-IR, and UV–Vis spectroscopy. XRD results confirmed the formation of cubic NiO with a preferred (111) orientation. Increasing Ba content led to a reduction in peak intensities and the introduction of lattice strain, indicating the insertion of Ba^{2+} ions into the NiO lattice. Optical measurements showed high transparency of the films in the visible region, while the direct band gap decreased from 3.55 eV to 3.13 eV as the Ba concentration increased. These findings highlight the potential applicability of Ba-doped NiO in various optoelectronic devices.

Keywords: *Thin films; NiO; Spray pyrolysis; FT-IR; XRD*
PACS: 68.55.-a, 81.15.-z

1. INTRODUCTION

In recent years, thin films have attracted significant attention due to their wide-ranging applications in electronics, optoelectronics, and energy storage systems [1, 2, 3, 4]. Among the various materials employed in these technologies, transparent conducting oxides (TCOs) have shown remarkable promise, as they uniquely combine electrical conductivity with optical transparency an essential requirement for modern devices [3].

Nickel oxide (NiO) is a particularly attractive p-type TCO owing to its abundance, low cost, and favorable physical properties [1, 2]. It crystallizes in a face-centered cubic (NaCl-type) structure and possesses a relatively wide band gap, typically ranging from 3.25 to 4.00 eV. NiO exhibits high chemical stability, strong adhesion to substrates, and good transparency across the visible spectrum [4, 5]. These characteristics make it suitable for a variety of applications, including antiferromagnetic components [5], p-type transparent layers [6, 7], display technologies [8], photovoltaic devices [9], and gas sensors [10].

Numerous deposition techniques have been employed to produce NiO thin films, notably sol–gel processing [11], PECVD , PLD [12, 13], and magnetron sputtering [14, 15]. Among these, spray pyrolysis stands out as a cost-effective and versatile technique. It offers simplicity, compatibility with large-area deposition, and does not require high-vacuum equipment [16, 17]. Films fabricated by spray pyrolysis generally exhibit good uniformity and strong adhesion to glass substrates, making this approach attractive for large-scale industrial applications.

Doping is a widely used strategy for tailoring the structural, optical, and electrical characteristics of NiO thin films. Previous studies have shown that dopants such as Fe can significantly enhance performance by inducing lattice modifications or generating new energy levels [18]. In this context, barium (Ba) is an interesting dopant candidate due to its large ionic radius, which can influence the NiO lattice and potentially modulate its optoelectronic behavior.

The aim of the present study is to investigate the influence of barium doping on the structural and optical properties of NiO thin films prepared via spray pyrolysis. By varying the Ba concentration, we examine how this modification affects crystallinity, band gap energy, defect states, and optical constants. The results presented here are expected to contribute to the development of NiO-based materials for advanced optoelectronic applications.

2. METHODS AND MATERIALS

2.1. Thin Film Preparation

Nickel oxide (NiO) thin films were synthesized using the spray pyrolysis technique with varying concentrations of barium (Ba) as a dopant. The Ba doping levels examined were 0, 2, 4, 6, and 8 at.% relative to Ni.

The precursor solutions were prepared by dissolving nickel nitrate hexahydrate $Ni(NO_3)_2 \cdot 6H_2O$ and barium nitrate $Ba(NO_3)_2$, each at a concentration of 0.2 M, in distilled water. For the doped samples, the Ba nitrate solution was mixed with the nickel nitrate solution in volumetric ratios corresponding to the desired Ba atomic percentages (at.%). Since

Cite as: M. Begui, M. Ghougali, East Eur. J. Phys. 1, 531 (2025), https://doi.org/10.26565/2312-4334-2026-1-61

both precursor solutions were prepared at the same molar concentration (0.2 M), the Ba atomic percentage is directly determined from the volumetric mixing ratio and calculated as

$$Ba(at.\%) = \frac{V_{Ba}}{V_{Ba} + V_{Ni}} \times 100 \quad (1)$$

where V_{Ba} and V_{Ni} denote the volumes of Ba and Ni precursor solutions, respectively. The resulting solutions were continuously stirred and heated to 60°C to ensure complete homogenization.

Clean glass substrates were used for film deposition. The substrates were first cleaned with ethanol, followed by rinsing with deionized water to remove surface contaminants. Deposition was performed using a spray nozzle positioned 30 ± 1 cm above the substrate surface. Using a thermocouple and a digital temperature controller, the substrate temperature was maintained at 500 ± 10°C. The precursor solution was sprayed at a controlled flow rate of 2 mL/min.

During spray pyrolysis, thermal decomposition of the metal nitrates resulted in the formation of NiO films on the glass substrates according to the reaction [19]:

$$2\,\mathrm{Ni(NO_3)_2} + 6\,\mathrm{H_2O} \rightarrow 2\,\mathrm{NiO} + 4\,\mathrm{NO_2}\uparrow + \mathrm{O_2}\uparrow + 6\,\mathrm{H_2O}\uparrow .$$

2.2. Characterization Methods

The structural characteristics of the deposited films were investigated using X-ray diffraction (XRD) with a benchtop powder diffractometer (Proto Manufacturing AXRD) employing Cu Kα radiation (λ = 1.54184 Å) at 30 kV and 30 mA.

To study the optical properties, including transmittance and band gap energy, UV–Vis spectrophotometry was performed using a Shimadzu 3101 PC spectrometer covering a broad wavelength range from 200 to 1100 nm.

Fourier-transform infrared spectroscopy (FTIR) was carried out using a Shimadzu IR–Infinity 1 spectrometer in the range of 400–2000 cm^{-1} to analyze the vibrational modes and confirm the chemical bonding within the films.

The thickness t of the deposited thin films was determined using optical methods based on transmittance data, with the results summarized in Table 2.

3. RESULTS AND DISCUSSION

3.1. Structural Properties

3.1.1. X-Ray Measurement. The XRD patterns of both undoped and Ba-doped NiO thin films are presented in Figure 1. Prominent diffraction peaks appear at $2\theta \approx 37.3°$, 43.2°, and 62.8°, corresponding to the (111), (200), and (220) planes of cubic NiO respectively,These are in good agreement with the ICDD PDF Card No. 47-1049, confirming the formation of a face-centered cubic (Fm-3m) phase with a (111) preferred orientation. In the 4% Ba-doped sample, an additional weak diffraction peak appears at $2\theta \approx 59.14°$, which does not correspond to any characteristic reflection of cubic NiO. This peak is therefore attributed to the formation of a secondary Ba-containing phase, likely arising from excess Ba incorporation during film growth. With increasing Ba concentration, the intensity of the NiO diffraction peaks decreases, indicating increased lattice distortion and a reduction in long-range crystalline order [20]. A slight shift of the (111) peak position toward lower 2θ angles is observed with Ba incorporation, reflecting changes in the lattice parameters due to dopant-induced strain [21].

3.1.2. Crystallite Size and Structural Parameters. Using Bragg's law and the Scherrer formula [22], the lattice parameter and crystallite size were calculated and are summarized in Table 1. The variation of crystallite size (D) and lattice parameter (a) as a function of Ba concentration is illustrated in Figure 2. At low Ba content (2 at.%), the crystallite size increases, indicating an initial improvement in grain growth. A sharp reduction in crystallite size is observed at 4 at.% Ba doping, which is attributed to increased lattice distortion and the onset of a secondary Ba-containing phase. With further increase in Ba concentration (6 and 8 at.%), the crystallite size remains relatively reduced, reflecting enhanced defect formation and dopant-induced strain. The lattice parameter shows a non-monotonic variation with Ba content, confirming that Ba incorporation significantly affects the crystal structure of NiO thin films. These results demonstrate that excessive Ba doping degrades the structural quality of NiO films.

The non-monotonic evolution of crystallite size can be explained by the significant ionic radius mismatch between Ba^{2+} (135 pm) and Ni^{2+} (69 pm) ions. At low Ba concentration (2 at.%), partial substitution of Ni^{2+} by Ba^{2+} may introduce moderate lattice distortion that enhances atomic diffusion during film growth, promoting grain coalescence and increasing crystallite size [23]. With further increase in Ba content, the large ionic size of Ba^{2+} generates substantial lattice strain and defect formation within the NiO matrix. When the Ba concentration approaches approximately 4 at.%, the solubility limit of Ba in NiO is likely reached, leading to dopant segregation at grain boundaries and the appearance of a secondary Ba-containing phase [24]. This segregation restricts grain growth and results in crystallite size reduction. Therefore, the structural behavior reflects a competition between diffusion-assisted grain growth at low doping levels and strain-induced grain refinement at higher Ba concentrations.

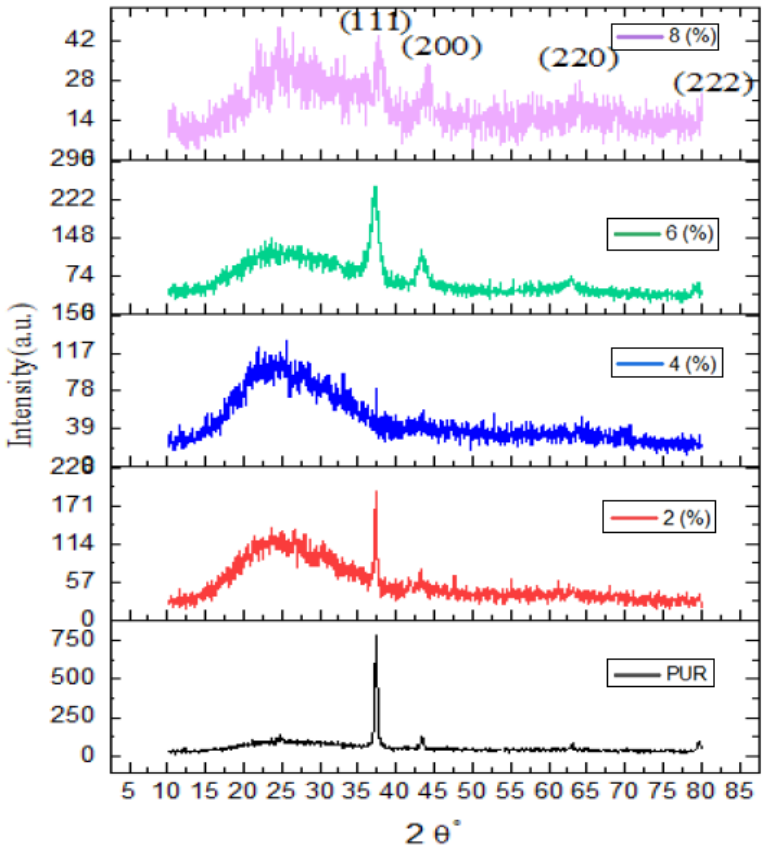

Figure 1. XRD patterns of Ba doped NiO thin films at different Ba concentrations.

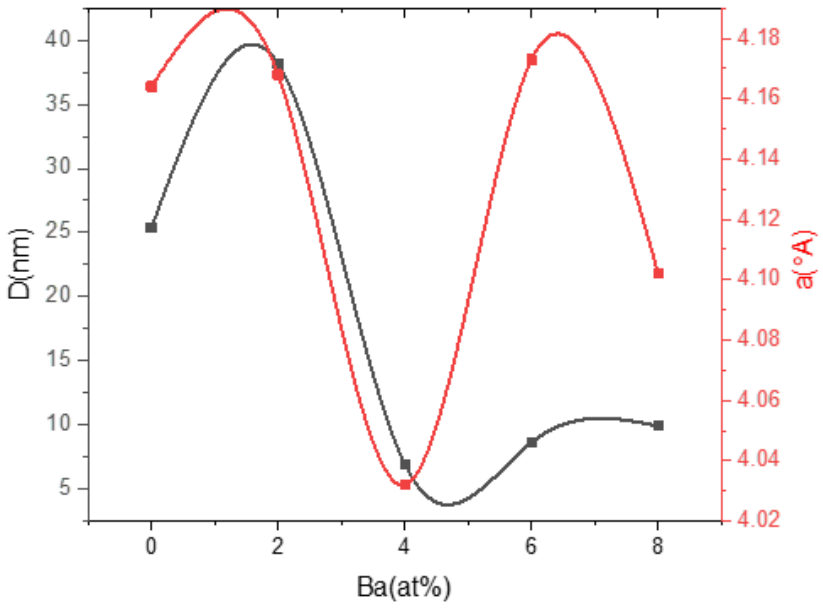

Figure 2. Variations of grain size, and lattice parameter as a function of Ba concentration.

Table 1. Structural parameters of undoped and Ba-doped NiO thin films, including diffraction angle (2θ), interplanar spacing (d_{hkl}), lattice constant (a), crystallite size (D), dislocation density (δ), and microstrain (ε).

Sample	2θ (deg)	d_{hkl} (Å)	(hkl)	a (Å)	FWHM (deg)	D (nm)	δ (10^{15} line/m^2)	Microstrain (ε)
NiO	37.249	–	(111)	–	–	–	–	–
(ICDD PDF	43.276	–	(200)	4.177	–	–	–	–
No. 47-1049)	62.879	–	(220)	–	–	–	–	–
	37.377	2.404	(111)					
Ba:NiO 0%	43.434	2.083	(200)	4.164	0.3306	25.36	1.54	0.00427
	63.113	1.473	(220)					
	37.339	2.407	(111)					
Ba:NiO 2%	43.335	2.088	(200)	4.168	0.2204	38.18	0.683	0.00285
	64.387	1.275	(220)					
Ba:NiO 4%	38.684	2.329	(111)	4.032	1.2210	6.91	20.9	0.0152
	59.142	–	Secondary phase	–	–	–	–	–
	37.317	2.409	(111)					
Ba:NiO 6 %	43.291	2.111	(200)	4.173	0.9742	8.65	13.4	0.0130
	62.817	0.042	(220)					
	38.027	2.368	(111)					
Ba:NiO 8%	44.057	2.055	(200)	4.102	0.8502	9.92	10.2	0.0110
	63.499	1.465	(220)					

3.2. FTIR Spectroscopy

Figure 3 displays the Fourier-transform infrared (FTIR) spectra obtained from both undoped and Ba-doped NiO thin films in the range of 400–2000 cm^{-1}. A prominent absorption band between 414–449 cm^{-1} corresponds to Ni–O stretching vibrations, confirming the presence of NiO. An additional band near 755–760 cm^{-1} is attributed to general metal–oxygen (M–O) bending vibrations [25].

These spectral features validate the formation of NiO and suggest that Ba doping does not fundamentally alter the Ni–O bonding environment, although minor shifts may indicate subtle structural perturbations.

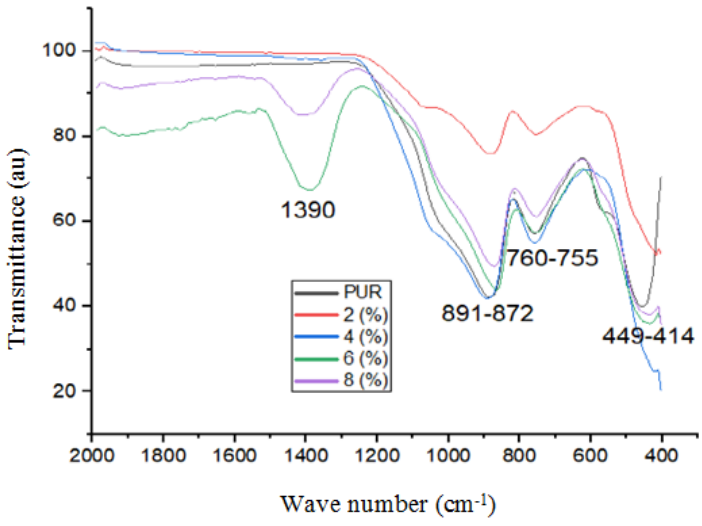

Figure 3. FTIR spectra of undoped and Ba-doped NiO thin films.

3.3. Optical Properties

3.3.1. Transmittance and Absorption. Figure 4 presents the transmittance spectra for all samples across the wavelength range of 300–900 nm. The undoped and lightly doped films (2% and 4%) exhibit transmittance values exceeding 60%, indicating high transparency. In contrast, films with higher Ba concentrations (6% and 8%) show reduced transparency, attributed to increased light absorption arising from dopant-induced defect states located near the conduction band edge.

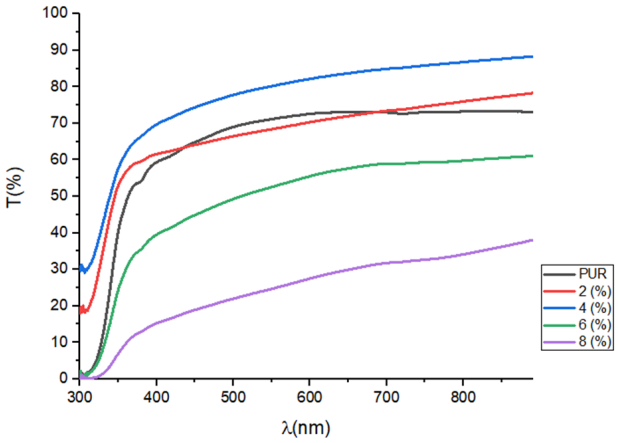

Figure 4. Transmittance spectra of NiO:Ba thin films.

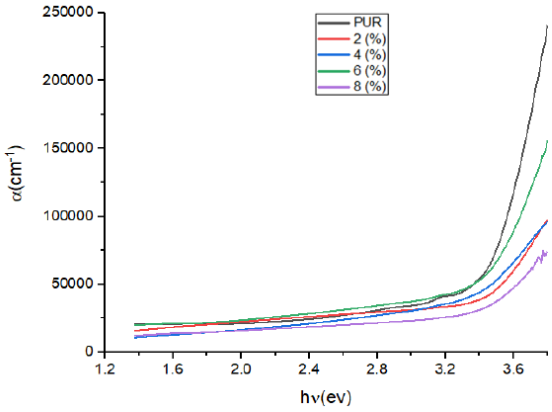

Figure 5. Absorption coefficient vs. photon energy for NiO:Ba films.

The absorption coefficient α was determined from the optical data of the thin films, taking into account both absorbance and film thickness. As illustrated in Figure 5, the absorption coefficient α increases progressively with rising Ba doping levels. This behavior indicates that the incorporation of barium enhances the films light absorption, which can be associated with modifications in the electronic band structure. The observed trend reflects the formation of additional energy levels or localized states within the material as Ba content increases, thereby facilitating greater photon absorption and effectively altering the optical response of the NiO thin films.

3.3.2. Energy of the Band Gap. The optical band gap E_g was estimated using the Tauc relation:

$$(\alpha h\nu)^n = A(h\nu - E_g), \tag{2}$$

where α is the absorption coefficient, $h\nu$ is the photon energy, A is a proportionality constant related to the transition probability, E_g is the optical band gap energy, and n depends on the nature of the electronic transition. For direct allowed transitions, $n = 2$ was used. Assuming a direct allowed transition for NiO, the band gap values were determined by extrapolating the linear region of the $h\nu$ plots to the energy axis, as shown in Figure 6. The band gap decreases from 3.55 eV (undoped) to 3.13 eV for the 8% Ba-doped film, indicating the formation of defect-related localized states and band tailing. This redshift in the absorption edge is a typical consequence of dopant-induced structural disorder.

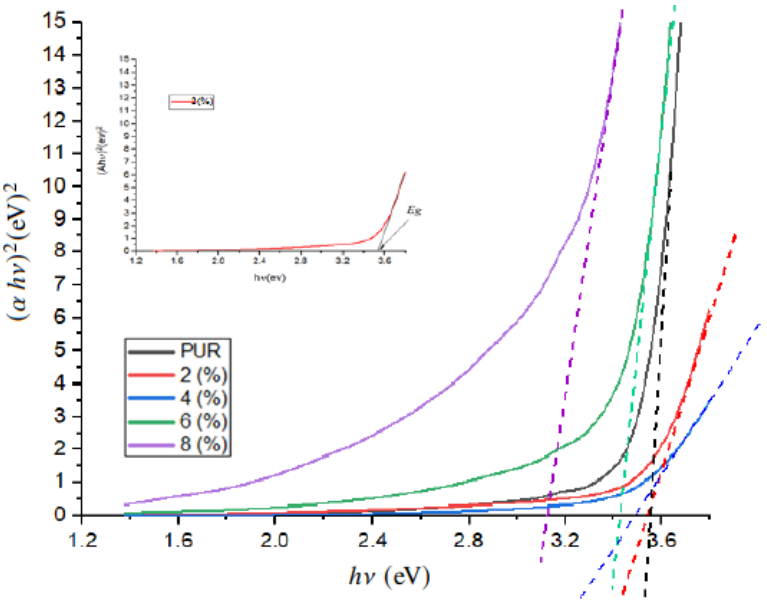

Figure 6. Tauc plots for band gap energy determination.

3.3.3. Urbach Energy (E_U). The Urbach energy E_U, which quantifies the extent of the tail of localized states in the band gap, was determined from the slope of the linear region in the $\ln(\alpha)$ versus photon energy $h\nu$ plot.

As shown in Figure 7 and Table 2, E_U increases with Ba doping (except at 6%), indicating that structural disorder and defect density become more pronounced at higher dopant concentrations. An inverse correlation is observed between E_g and E_U, consistent with typical behavior in disordered semiconductor systems.

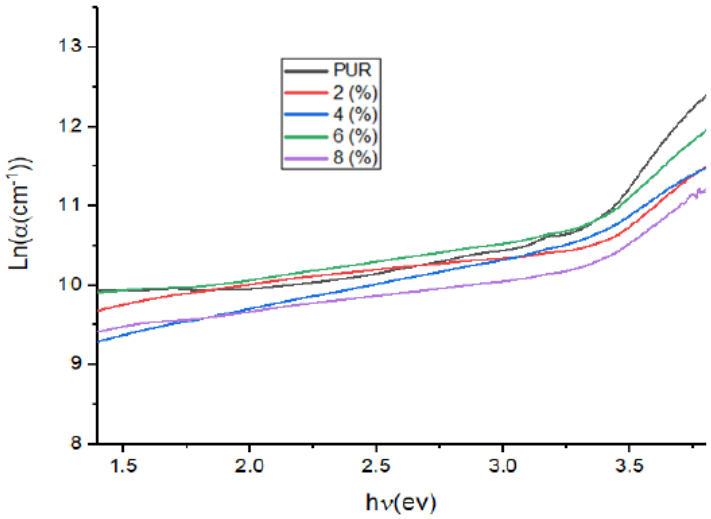

Figure 7. Urbach plots of NiO:Ba thin films.

Table 2. Values of thickness t, optical band gap energy E_g,and Urbach energy E_U of the undoped and Ba-doped NiO thin films

	$t(nm)$	$E_g(eV)$	$E_U(eV)$
Pure NiO:Ba	150.85	3.55	0.235
NiO:Ba(2%)	155.81	3.54	0.414
NiO:Ba(4%)	117.34	3.49	0.442
NiO:Ba(6%)	246.81	3.42	0.341
NiO:Ba(8%)	805.81	3.13	0.413

3.3.4. Extinction Coefficient and Refractive Index. The extinction coefficient k was determined from the absorption coefficient α and the wavelength λ as outlined in [26]. As shown in Figure 8, k increases with Ba doping, reflecting enhanced optical absorption.

Similarly, the refractive index n was calculated based on the reflectance R and the extinction coefficient, following the method described in [26]. Figure 9 shows that the refractive index n increases at lower photon energies and sharply decreases beyond approximately 3.4 eV, likely due to interband electronic transitions. The 8% Ba-doped sample exhibits anomalous behavior, which may be attributed to excessive defect formation.

3.3.5. Dielectric Function. The real (ε_r) and imaginary (ε_i) parts of the dielectric constant were calculated using the following relations [26]:

$$\varepsilon_r = n^2 - k^2 \tag{3}$$

$$\varepsilon_i = 2nk \tag{4}$$

Figure 10 and Figure 11 illustrate the variation of the real (ε_r) and imaginary (ε_i) parts of the dielectric constant as a function of photon energy ($h\nu$) for different Ba concentrations. For lower doping levels (2% and 4%), both components generally increase with photon energy and Ba content. However, at the highest doping concentration (8%), both ε_r and ε_i exhibit a significant decrease, particularly in the high-energy region above 2.5 eV. Throughout most of the measured range, the real part ε_r remains larger than the imaginary part ε_i, suggesting that light propagation is the dominant process compared to energy loss in these films. These results indicate that Ba doping effectively modifies the dielectric response, though the trend non-linearly depends on the Ba concentration.

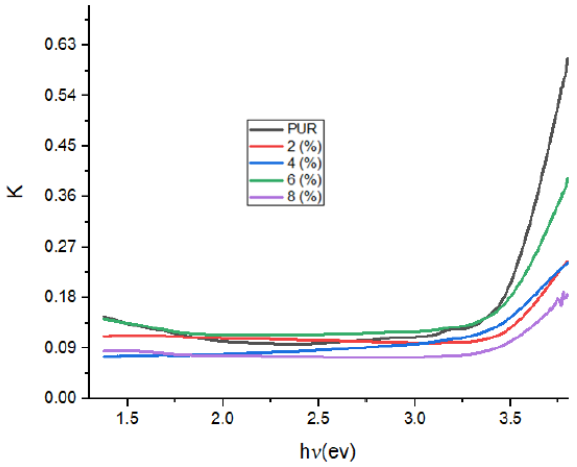

Figure 8. Effect of doping on extinction coefficient (k).

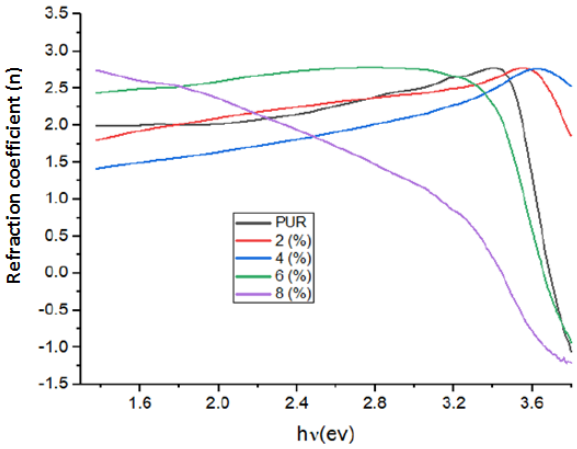

Figure 9. Effect of doping on refractive index (n).

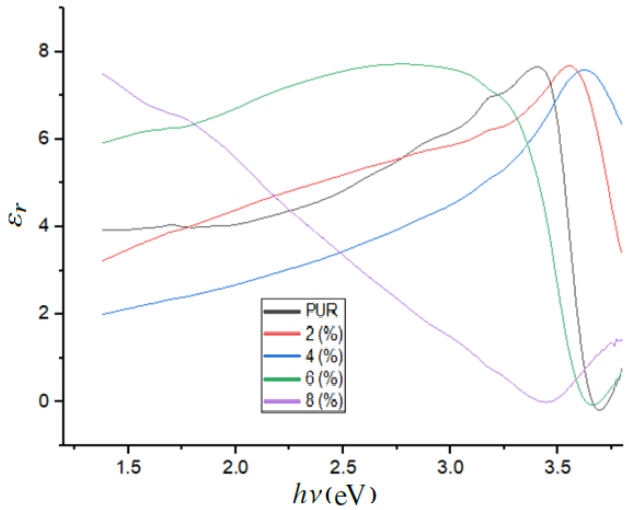

Figure 10. Real part of the dielectric constant vs. photon energy.

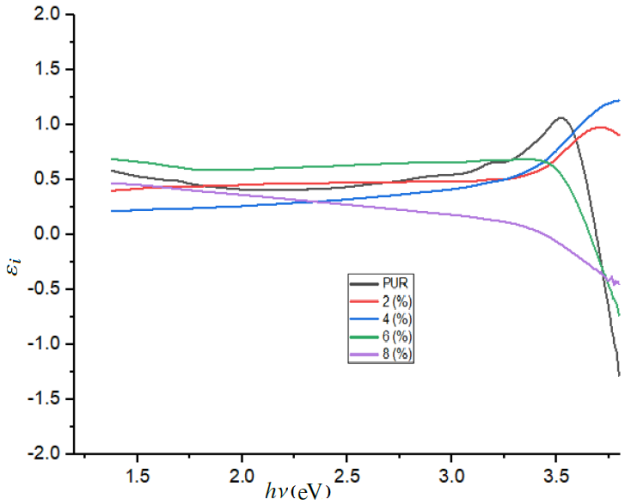

Figure 11. Imaginary part of the dielectric constant vs. photon energy.

4. CONCLUSIONS

NiO thin films, both undoped and Ba-doped, were successfully synthesized by the spray pyrolysis technique. X-ray diffraction analysis confirmed the formation of a single-phase cubic NiO structure with space group $Fm\bar{3}m$, characterized by dominant reflections along the (111), (200), and (220) planes. All films exhibited a preferred orientation along the (111) direction. The incorporation of Ba significantly influenced the structural properties of NiO, as evidenced by changes in peak intensities, lattice parameters, and crystallite size.

A detailed structural analysis revealed that low Ba doping slightly improves crystallinity, whereas higher Ba concentrations induce lattice distortion and structural disorder. The crystallite size shows a non-monotonic dependence on Ba content, increasing at low doping levels and decreasing markedly at higher concentrations due to enhanced strain and defect formation. In the 4% Ba-doped sample, the appearance of an additional weak diffraction peak was attributed to a secondary Ba-containing phase, indicating the solubility limit of Ba in the NiO lattice under the present deposition conditions. These results demonstrate that excessive Ba incorporation deteriorates the structural order of the films.

FTIR measurements confirmed the formation of Ni–O bonds in all samples, indicating successful oxide formation. Optical transmittance spectra in the 300–900 nm range revealed high transparency for all films, with a maximum transmittance of approximately 88% observed for the 4% Ba-doped sample. The optical band gap exhibited a gradual redshift with increasing Ba concentration, which is attributed to the introduction of defect-related localized states and increased structural disorder.

Furthermore, key optical constants, including the absorption coefficient, extinction coefficient, refractive index, and dielectric functions, were systematically evaluated and found to be strongly dependent on Ba doping. These variations further confirm the role of Ba incorporation in modifying the optical response of NiO thin films.

Overall, this study demonstrates that Ba doping provides an effective approach to systematically modulate the

structural and optical properties of NiO thin films. While moderate Ba incorporation can enhance certain optical characteristics, excessive doping leads to structural degradation. These findings highlight the potential of Ba-doped NiO thin films for optoelectronic applications such as transparent electrodes, photovoltaics, and gas sensors. Future work will focus on electrical and optoelectrical characterization to further assess their suitability for device applications.

ORCID

Mohamed Begui, https://orcid.org/0000-0001-8378-5058; **Mebrouk Ghougali**, https://orcid.org/0000-0003-0496-4555

REFERENCES

[1] M. Ghougali, O. Belahssen, and A. Chala, "Investigation of the Properties of NiO Thin Films Prepared by Spray Pyrolysis Technique," Journal of Nano- and Electronic Physics, **8**(4), 04059 (2016).

[2] O. Belahssen, M. Ghougali, and A. Chala, "Structural and Optical Properties of Nickel Oxide Thin Films Prepared by Spray Pyrolysis," Journal of Nano- and Electronic Physics, **10**(2), 02039 (2018). https://doi.org/10.21272/jnep.10(2).02039

[3] M. Ghougali, O. Belahssen, and A. Chala, "Effect of Substrate Temperature on the Properties of NiO Thin Films," Journal of Nano- and Electronic Physics, **9**(3), 03043 (2017). https://doi.org/10.21272/jnep.9(3).03043

[4] R. Sharma, A. D. Acharya, S. B. Shrivastava, T. Shripathi, and V. Ganesan, "Effect of thickness on structural, optical and electrical properties of NiO thin films," Optik, **125**(22), 6751–6756 (2014). https://doi.org/10.1016/j.ijleo.2014.07.104

[5] L. Cattin, B. Reguig, A. Khelil, M. Morsli, K. Benchouk, and J. Bernede, "Properties of NiO thin films deposited by chemical spray pyrolysis using different precursor solutions," Applied Surface Science, **254**(18), 5814–5821 (2008). https://doi.org/10.1016/j.apsusc.2008.03.071

[6] E. Fujii, A. Tomozawa, H. Torii, and R. Takayama, "Preferred orientations of NiO films prepared by plasma-enhanced metalorganic chemical vapor deposition," Japanese Journal of Applied Physics, **35**(3A), L328 (1996). https://doi.org/10.1143/JJAP.35.L328

[7] H. Sato, T. Minami, S. Takata, and T. Yamada, "Transparent conducting p-type NiO thin films prepared by magnetron sputtering," Thin Solid Films, **236**(1-2), 27–31 (1993). https://doi.org/10.1016/0040-6090(93)90636-4

[8] V. H. López-Lugo, M. García-Hipólito, A. Rodríguez-Gómez, and J. C. Alonso-Huitrón, "Fabrication of Li-Doped NiO Thin Films by Ultrasonic Spray Pyrolysis and Its Application in Light-Emitting Diodes," Nanomaterials, **13**(4), 197 (2023). https://doi.org/10.3390/nano13010197

[9] K. Yoshimura, T. Miki, and S. Tanemura, "Nickel Oxide Electrochromic Thin Films Prepared by Reactive DC Magnetron Sputtering," Japanese Journal of Applied Physics, **34**(5R), 2440 (1995). https://doi.org/10.1143/JJAP.34.2440

[10] H. L. Chen, Y. M. Lu, and W. S. Hwang, "Characterization of sputtered NiO thin films," Surface and Coatings Technology, **198**(1-3), 138–142 (2005). https://doi.org/10.1016/j.surfcoat.2004.10.032

[11] I. Hotovy, J. Huran, *et al*. "The influences of preparation parameters on NiO thin film properties for gas sensing application," Sensors and Actuators B: Chemical, **78** (1–3), 126–132 (2001). https://doi.org/10.1016/S0925-4005(01)00802-4

[12] US. Joshi, R. Takahashi, Y. Matsumoto, and H. Koinuma, "Structure of NiO and Li-doped NiO single crystalline thin layers with atomically flat surface," Thin Solid Films, **486**(1-2), 214-217 (2005). https://doi.org/10.1016/j.tsf.2004.11.219

[13] Y. Kakehi, S. Nakao, K. Satoh, and T. Kusaka, "Room-temperature epitaxial growth of NiO (1 1 1) thin films by pulsed laser deposition," Journal of Crystal Growth, **237-239**, 591-595 (2002). https://doi.org/10.1016/S0022-0248(01)01964-9

[14] H.-L. Chen, Y.-M. Lu, and W.-S. Hwang, "Thickness dependence of electrical and optical properties of sputtered NiO thin films," Thin Solid Films, **498**(1), 266–270 (2006). https://doi.org/10.1016/j.tsf.2005.07.124

[15] Zhi-Zhen Ye, *et al*. "Preparation and characterization of p-type ZnO films by DC reactive magnetron sputtering," Journal of Crystal Growth, **253**(1), 258–264, (2003). https://doi.org/10.1016/S0022-0248(03)01007-8

[16] B.A. Reguig, A. Khelil, L. Cattin, M. Morsli, and J.C. Bernède, "Properties of NiO thin films deposited by intermittent spray pyrolysis process," Applied Surface Science, **253**(9), 4330-4334, (2007). https://doi.org/10.1016/j.apsusc.2006.09.046

[17] T.H. Noh, W. Y. Jeung, I. K. Kang, S. H. Shin, and J. J. Lee, "Magnetic properties of Pr-Fe-B alloy powders prepared by mechanical grinding," Journal of Applied Physics, **70**(10), 6591–6593 (1991). https://doi.org/10.1063/1.349867

[18] D. Amaranatha Reddy, A. Divya, G. Murali, and R.P. Vijayalakshmi,"Synthesis and optical properties of Cr doped ZnS nanoparticles capped by 2-mercaptoethanol," Physica B, **406**(10), 1944–1949 (2011). https://doi.org/10.1016/j.physb.2011.02.062

[19] W. Brockner, C. Ehrhardt, and M. Gjikaj, "Thermal decomposition of nickel nitrate hexahydrate $Ni(NO_3)_2{\cdot}6H_2O$, in comparison to $Co(NO_3)_2{\cdot}6H_2O$ and $Ca(NO_3)_2{\cdot}4H_2O$," Thermochimica Acta, **456**(1), 64–68 (2007). https://doi.org/10.1016/j.tca.2007.01.031

[20] L. R.Singha, and R.K.L. Singh, "Effect of Dopant Concentration on Structural Properties of Chemical Bath Deposited Mn-Doped PbS Nanocrystalline Thin Films," Chalcogenide Letts, **17**(7), 375-384(2020)

[21] M. Ghougali, *et al*, "Investigation of the physical properties of nanostructured CO:NiO thin films," Chalcogenide Letters, **18**, 765–772 (2021). https://doi.org/10.15251/CL.2021.1812.765

[22] A. Patterson, "The Scherrer Formula for X-Ray Particle Size Determination," Physical Review, **56**(10), 978 (1939). https://doi.org/10.1103/PhysRev.56.978

[23] Kiprotich, Nancy, *et al*. "Effects of Tin Doping Concentration on the Structural and Optical Properties of Cadmium Oxide Nanoparticles," Advances in Materials, **14**(2), 55–64 (2025). https://doi.org/10.11648/j.am.20251402.13

[24] M. Kindelmann, *et al*., "Segregation-controlled densification and grain growth in rare earth-doped Y_2O_3", Journal of the American Ceramic Society, **104**(10), 4946–4959 (2021). https://doi.org/10.1111/jace.17907

[25] R. Barir, B. Benhaoua, S. Benhamida, *et al*., "Effect of Precursor Concentration on Structural Optical and Electrical Properties of NiO Thin Films Prepared by Spray Pyrolysis," Journal of Nanomaterials, **2017**, 5204639 (2017). https://doi.org/10.1155/2017/5204639

[26] M. E. Begum, M. Chowdhury, and M. B. Islam, "Structural, morphological and optical characterizations of spray pyrolyzed nickel oxide thin films," Results in Materials, **14** , 100265 (2022). https://doi.org/10.1016/j.rinma.2022.100265

ВПЛИВ ЛЕГУВАННЯ БАРІЄМ НА СТРУКТУРНІ ТА ОПТИЧНІ ВЛАСТИВОСТІ ТОНКИХ ПЛІВОК NiO

Мохамед Бегуі[1], **Мебрук Гудалі**[1,2]

[1]*Факультет точних наук, група фотоніки, дослідницький підрозділ розвитку відновлюваної енергетики в посушливих зонах (UDERZA), Університет Ель-Уед, Ель-Уед, Алжир*

[2]*Факультет точних наук, лабораторія LEVRES, Університет Ель-Уед, 39000 Ель-Уед, Алжир*

У цьому дослідженні досліджується вплив легування барієм (Ba) на структурні та оптичні властивості тонких плівок оксиду нікелю (NiO), синтезованих за допомогою розпилювального піролізу. Плівки NiO з концентрацією Ba 0%, 2%, 4%, 6% та 8% були проаналізовані за допомогою рентгенівської дифракції, ІЧ-спектроскопії з перетворенням Фур'є та УФ-видимої спектроскопії. Результати рентгенівської дифракції підтвердили утворення кубічного NiO з переважною (111) орієнтацією. Збільшення вмісту Ba призвело до зменшення інтенсивності піків та появи деформації решітки, що вказує на впровадження іонів Ba^{2+} у решітку NiO. Оптичні вимірювання показали високу прозорість плівок у видимій області, тоді як ширина забороненої зони зменшилася з $3,55\,eV$ до $3,13\,eV$ зі збільшенням концентрації Ba. Ці результати підкреслюють потенційну можливість застосування NiO легованого Ba в різних оптоелектронних пристроях.

Ключові слова: *тонкі плівки; NiO; розпилювальний піроліз; ІЧ-спектроскопія з перетворенням Фур'є; рентгенівська дифракція*